Available online at www.sciencedirect.com
ScienceDirect
Advances in Space Research 39 (2007) 1706–1714
ADVANCES IN SPACE RESEARCH (a COSPAR publication)
www.elsevier.com/locate/asr

How to improve the maps of magnetic helicity injection in active regions?

Etienne Pariat [a,b,*], Pascal Démoulin [a], Alexander Nindos [c]

[a] LESIA, Observatoire de Paris-Meudon, 92195 Meudon Cedex, France
[b] Université Paris 7 – Denis Diderot, 75251 Paris Cedex 05, France
[c] Section of Astrogeophysics, Department of Physics, University of Ioannina, GR-45110, Greece

Received 31 October 2006; received in revised form 6 February 2007; accepted 12 February 2007

Abstract

Magnetic helicity, a topological quantity which measures the twist, the writhe and the shear of a magnetic field, has recently appeared as a key quantity to understand some mechanisms of the solar activity such as Coronal Mass Ejections and flare onset. It is thus becoming of major importance to be able to compute magnetic helicity in active regions. Computing photospheric maps of the injection of magnetic helicity provides new spatial information that helps us to understand basic properties of solar activity, such as where and how magnetic helicity is injected.

Several helicity flux density maps have been published for different active regions. Unfortunately, the classical helicity flux density is not a correct physical quantity and it does induce spurious signals (fake polarities) which mask the real injection of helicity. To map the real helicity injection, the knowledge of the complete connectivity of the field lines is fundamental. Even without the connectivity, improved helicity flux density maps can be derived. They have fake polarities which are lower by more than a factor 10 than the previous incorrect maps. Rather than a mixture of negative and positive injection patterns, they show almost unipolar injection on the active region scale. This leads to a completely new way of understanding the dynamics of active regions, in the frame of magnetic helicity studies.

Keywords: Sun: magnetic fields; Sun: photosphere; Sun: corona

1. Introduction

1.1. Magnetic helicity

Magnetic helicity has initially been defined by Elsasser (1956) as a particularly interesting volume integral, one of the few invariant in ideal magnetohydrodynamic (MHD). Later, Moffatt (1969) has demonstrated that magnetic helicity is related to the geometrical properties of magnetic flux tubes: magnetic helicity is the sum of the Gauss linking number of every couple of magnetic flux tubes multiplied by their axial fluxes (the Gauss linking number is an integral which gives the number of links between two closed curves, i.e., the number of times one curve is going through the other: in the solar case the curves correspond to the axes of the flux tubes). Using the concept of magnetic helicity in solar physics is not straightforward since magnetic helicity is not gauge independent when the volume considered is not a magnetic volume. Important progress has been made by Berger and Field (1984) who defined the relative magnetic helicity: it quantifies how the magnetic field is sheared and/or twisted compared to a reference field, usually taken to be the potential field (which corresponds to the lowest energy state for a given distribution of the normal field component at the boundary).

* Corresponding author. Address: LESIA, Observatoire de Paris-Meudon, 92195 Meudon Cedex, France. Tel.: +33 145077756.
E-mail address: etienne.pariat@obspm.fr (E. Pariat).

0273-1177/$30 © 2007 Published by Elsevier Ltd on behalf of COSPAR.
doi:10.1016/j.asr.2007.02.047

Observations of the solar atmosphere show the existence of sheared, even helical magnetic structures. Such structures are often associated with flares, eruptive filaments and coronal mass ejections (CMEs). Magnetic helicity thus appears as a key element in a large number of coronal phenomena. A particularly important question is the role that helicity plays to explain the origin of CMEs. Magnetic helicity is an extremely well conserved quantity in the solar corona, even during reconnection – this has been shown from theoretical (Berger, 1984), experimental (Ji, 1999) and numerical arguments (Antiochos et al., 1999; Linton and Antiochos, 2005). Because of this conservation property, it has been suggested that CMEs can be viewed as the needed phenomena that allow the Sun to eject the helicity which is constantly injected through the photosphere, so CMEs would avoid the endless accumulation of helicity in the corona (Rust, 1994; Low, 1996). For all the above reasons, an increasing numbers of works have recently focused in magnetic helicity (see reviews by Brown et al., 1999; Berger, 2003; Démoulin, 2007).

The direct computation of helicity in the corona requires knowledge of the magnetic field connectivity in the entire studied volume, but since magnetic field measurements are mainly made at the photospheric level, the most common way to estimate magnetic helicity is through the computation of the time integral of the photospheric helicity rate (or total flux). How precise are these estimations is a subject of present active research (see the critical review by Démoulin, 2007).

A complementary aspect is to understand the spatial distribution of the photospheric injection of magnetic helicity. For example, do we have injection of both sign of helicity at different locations within the same AR? The answer has consequences for the dynamo; since magnetic helicity is a well preserved quantity, we will have clues on the way the magnetic flux was distorted by the plasma flow, so how the field was amplified and twisted. The answer to the above question has also consequences for coronal physics, in particular for flares and CMEs. Are they the consequence of reconnection of flux tubes having opposite helicity, which would permit a larger amount of magnetic energy to be released? Or is the injection of helicity mostly of a given sign? If the latter is the case, then magnetic helicity accumulates in the corona, and then could it finally lead to CMEs? Moreover, is magnetic helicity mostly injected during the emergence phase of ARs? How the highly sheared, and probably twisted, magnetic configurations supporting quiescent filaments are formed? How they get such important amount of helicity? Is it injected from the large scales (e.g., differential rotation), or from the local scales (e.g., close to the magnetic inversion line)? Thus, in order to answer many key questions of solar physics, the study of the helicity rate is not sufficient and we need to estimate the helicity flux per unit surface, or flux density. The aim of this paper is to show how we can compute more reliable maps of helicity injection.

1.2. Previous magnetic helicity flux density estimations

The helicity rate $\mathrm{d}H/\mathrm{d}t$ through a planar surface S can be written as (Berger and Field, 1984):

$$\frac{\mathrm{d}H}{\mathrm{d}t} = 2\int_S [(\mathbf{A}_\mathrm{p}\cdot\mathbf{B})v_\mathrm{n} - (\mathbf{A}_\mathrm{p}\cdot\mathbf{v})B_\mathrm{n}]\mathrm{d}S, \tag{1}$$

where $\mathbf{A}_\mathrm{p}$ is the vector potential of the potential magnetic field (without electric currents); $\mathbf{B}$, $\mathbf{v}$, B_n and v_n, respectively, represent the magnetic field, the plasma velocity field and their projection along the direction normal to the surface.

For the solar photosphere, the first term of Eq. (1) corresponds to injection of helicity by emergence of magnetic flux into the corona and the second term, called the shear term, is the rate of helicity due to motions parallel to the photosphere (like differential rotation). To compute them it is necessary to derive the photospheric plasma velocity field $\mathbf{v}$. This is done with local correlation tracking (LCT) methods. Since only horizontal velocities are deduced from the temporal evolution of B_n by LCT, it has been believed that only the shear term could be derived. However, any LCT method estimates the velocity of the flux tube position, $\mathbf{u}$, in the photosphere and not the plasma velocity $\mathbf{v}$. Démoulin and Berger (2003) have shown that the rate of helicity can be written as

$$\frac{\mathrm{d}H}{\mathrm{d}t} = -2\int_S (\mathbf{A}_\mathrm{p}\cdot\mathbf{u})B_\mathrm{n}\mathrm{d}S. \tag{2}$$

Thus using LCT, it is not possible to discriminate the shear term from the emergence term, but the total helicity rate is directly estimated.

It is also important to study the spatial distribution of the injection by considering the integrand of Eq. (2)

$$G_\mathrm{A} = -2(\mathbf{A}_\mathrm{p}\cdot\mathbf{u})B_\mathrm{n}. \tag{3}$$

In previous studies of active regions, G_A has been used extensively to monitor the spatial distribution of magnetic helicity flux density (Chae, 2001; Chae et al., 2001, 2004; Kusano et al., 2002; Nindos and Zhang, 2002; Nindos et al., 2003; Maeshiro et al., 2005; Moon et al., 2002a,b). However, in Pariat et al. (2005, 2006), we showed that G_A is not a real helicity flux density and that its properties generate intense artificial polarities of both signs. This is due to the presence of the vector potential which is not a physical quantity.

The aim of this paper is to present new definitions of helicity flux density, to describe their theoretical properties, and their implications on observations. In particular, we wish to demonstrate that thinking in terms of connectivity can improve our understanding of the helicity injection process. Section 2, summarizes how much G_A can be strongly misleading, and how a new definition, G_θ, is not subject to important fake polarities. In Section 3, we show that G_θ nevertheless creates some low-intensity fake polarities and we introduce an improved definition: G_Φ. Finally in Section 4, a tricky observational example, where G_θ

creates strong fakes signal, is analyzed in details. We show how, even without the complete knowledge of the field line connectivity, it is possible to have an idea of the spatial distribution of the helicity injection.

2. Helicity injection maps: from G_A to G_θ

2.1. Problems with G_A

The fact that G_A creates fakes polarity can be illustrated immediately with a very simple example. Let us consider a simple circular magnetic region (with $B_n > 0$) moving with any translational motion with a constant velocity $\mathbf{u}$ as in Fig. 1 (left panel). Here, the rate of helicity is null since no field line is twisted, sheared or braided due this motion. Locally, at each point, one expect that the helicity flux density is null. Nevertheless when computing G_A non-null terms appear. Indeed, in the classical Coulomb gauge, the vector field $\mathbf{A}_p$ is toroidal (see arrows in the top right panel of Fig. 1), while $\mathbf{u}$ is constant. Due to the scalar product in Eq. (3), G_A is positive in one half of the region, and negative in the other half (see Fig. 1).

The total helicity rate is null: the integration of G_A over the surface gives the expected result. Nevertheless G_A is non-null even with simple flows which do not input any magnetic helicity to the coronal field! G_A introduces artificial polarities of both signs with most flow patterns. Indeed, we cannot simply take the integrand of the helicity rate and consider it as a physical quantity since the helicity rate involves in fact a double integration over the surface (one integration is hidden in the computation of the vector potential).

In order to get rid of the most significant spurious signals, we suggested to substitute G_A by another definition of the helicity flux density, G_θ (Pariat et al., 2005)

$$G_\theta(\mathbf{x}) = -\frac{B_n(\mathbf{x})}{2\pi}\int_{S'}\frac{d\theta(\mathbf{x}-\mathbf{x}')}{dt}B_n(\mathbf{x}')dS', \quad (4)$$

where $d\theta/dt$ is the angular velocity of the vector $\mathbf{x}-\mathbf{x}'$ relatively to a given direction

$$\frac{d\theta(\mathbf{x}-\mathbf{x}')}{dt} = \frac{((\mathbf{x}-\mathbf{x}')\times(\mathbf{u}-\mathbf{u}'))_n}{(\mathbf{x}-\mathbf{x}')^2}. \quad (5)$$

Using G_θ instead of G_A strongly modifies the observed pattern of helicity injection. For any translational motion, since all points have the same velocity, the rotation rate $d\theta/dt$ of each pair of points is null and thus no helicity density will appear. From the G_θ map, the interpretation of the zero helicity injection is obvious (Fig. 1).

2.2. Applications of G_θ to observations

In Pariat et al. (2006), we compared G_A and G_θ maps of several actives regions. These active regions had previously been studied in detail by Nindos et al. (2003). We used 1-min cadence and 96-min cadence MDI data to study the helicity flux density given by these two definitions. The same data are used to compare G_A and G_θ maps.

The MDI data provided only the longitudinal (along the line of sight) component of the magnetic field and we assume that the photospheric magnetic field was vertical. The vertical field component, B_n, was then directly equal to the longitudinal field divided by the cosine of the heliocentric angle of the active region. The vector potential of the potential field, $\mathbf{A}_p$, was derived from B_n by fast Fourier transform method, following Chae (2001). The velocity field of the footpoints of the flux tubes, $\mathbf{u}$, was estimated by applying the LCT method to the longitudinal magnetograms. The used LCT parameters were $\omega = 7.5''$ for the width of the apodizing window function and $\Delta T = 15$–20 min for the time interval between a pair of images. To compute G_θ , we only needed to know B_n and $\mathbf{u}$. Since the vector potential is not required here, G_θ is not affected by the errors induced by the discrete Fourier transform when computing $\mathbf{A}_p$.

The comparison of G_A and G_θ maps shows that G_A indeed creates strong fake helicity flux polarities, due to

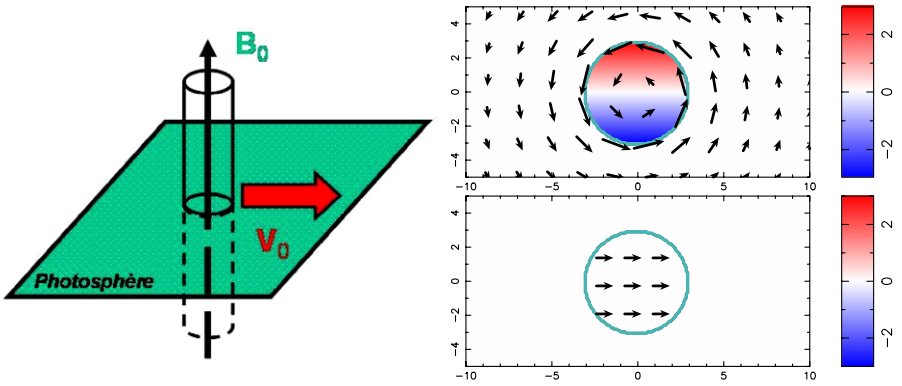

Fig. 1. Left: sketch of the considered motion: a single positive magnetic region (flux tube) executing a simple translational (global) motion towards the right. Right: maps of G_A (top panel) and of G_θ (bottom panel). The gray levels show the strength of G_A and G_θ with middle gray being 0, lighter gray (red) positive, and darker gray (blue) negative. In the top panel the arrows represent the vector potential $\mathbf{A}_p$. In the bottom panel they correspond to the velocity field $\mathbf{u}$. These maps have been computed with a uniform field component B_n within the magnetic polarity. (For interpretation of the references in color in this figure legend, the reader is referred to the web version of this article.)

the translational motions of magnetic polarities. With G_θ these spurious signals disappear: the non-dominant polarities of the helicity flux density are suppressed and the intensities of the dominant polarities are lowered (Pariat et al., 2006).

The total and signed helicity rate computed using G_A and G_θ were also compared. One expects theoretically that the total rates should be equal, but some differences do exist between dH_A/dt and dH_θ/dt in our data. These differences do not have a preferential sign and thus tend to become small when the data are time-averaged. As pointed by Chae et al. (2007), it is worth noticing that the computation of dH_A/dt and dH_θ/dt do not assume the same boundary conditions. The Fourier transform method adopted by Chae (2001) assumes that the flux distribution is periodically repeated outside the computation box. Computing dH_θ/dt implicitly assumes that there is no magnetic flux distribution outside the region of interest. This difference accounts partly for the differences observed between dH_A/dt and dH_θ/dt which could be has large as $\approx 10\%$. Moreover G_A has more intense polarities of opposite signs. Then integrating G_A implies the cancellation of important quantities, which in turn introduces additional errors. Concerning the unsigned rates, the non-dominant helicity rate with G_θ is strongly reduced compared with G_A and it has a more homogenous time variation, suggesting that it is dominated by noise.

For all five active regions that we studied in Pariat et al. (2006), the pattern of the helicity injection is much more homogeneous in G_θ maps than in G_A maps. This has several implications concerning the physics of the generation of magnetic helicity in the solar interior and of its transport in the convection zone (see review of Brandenburg and Subramanian, 2005). The theory will have to explain such observed features. Also such observations put constraints on the viability of some models of solar flares and CMEs where the eruption is triggered by the annihilation of opposite-sign magnetic helicity (Kusano et al., 2004).

3. Helicity injection maps: from G_θ to G_Φ

Even if G_θ strongly improves the estimation of magnetic helicity density, we can still find configurations where G_θ also produces fake signals.

For example, let us consider an arcade formed of a single flux tube. Let us consider that the footpoints rotate in opposite directions so that the flux tube rotates as a whole but does not increase its twist (see Fig. 2, top left). The velocity at a point of the flux tube is given by $\mathbf{v} = \boldsymbol{\Omega} \times \boldsymbol{\rho}$, with $\boldsymbol{\Omega}$ the rotation vector, which is directed along the axis of the flux tube, and with $\boldsymbol{\rho}$, the vector formed by the considered point and its orthogonal projection along the axis. Even if no helicity is injected in the flux tube, G_θ polarities of opposite sign appear at each footpoint (Fig. 2, top right).

However, generally G_θ parasitic helicity flux density polarities are much fainter than the G_A ones. In the case of Fig. 2, the polarities induced by G_A have an absolute intensity about 0.15, twice bigger than those induced by G_θ (see scale on the left of the G_θ map), but this is an extreme case. Previously, in the case of the emergence of a twisted flux tube, we estimated that these spurious polarities mask the real injected helicity when the number of turns of the twisted flux tube is lower than a few tenths of a turn. With G_θ the threshold in the number of turns is ten times lower than with G_A . In other theoretical examples, designed to represent the main characteristics features of observations, it was also shown that G_θ has fake polarities at least 10 times less intense than G_A (Pariat et al., 2005). Thus with G_θ we should be able to correctly analyze the injection of helicity of flux tubes having a significant amount of twist (a few tenths of turns).

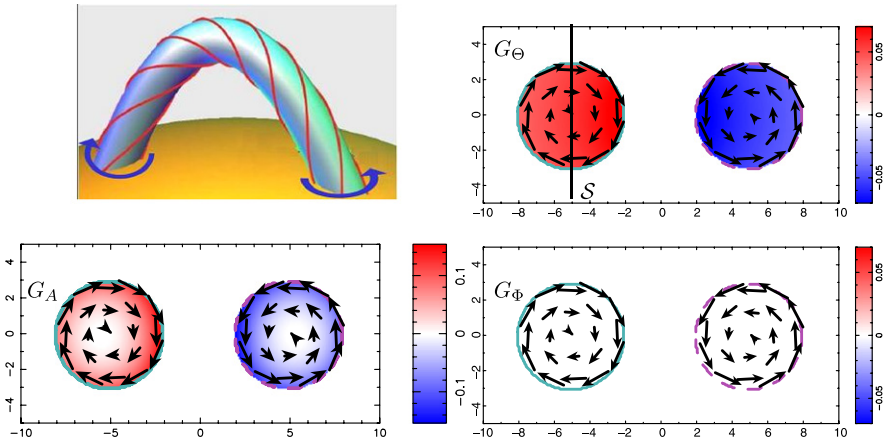

Fig. 2. Top left: sketch of a magnetic flux tube rotating as a whole (adapted from Berger, 1999). The number of turns of the field line is equal to 1. The other panels represent the photospheric maps of the helicity injection for this flux tube: G_A (bottom left), G_θ (top right) and G_Φ (bottom right). The arrows represent the velocity field $\mathbf{u}$. The gray levels show the strength of G_A , G_θ , and G_Φ with middle gray being 0, lighter gray (red) positive, and darker gray (blue) negative, with the magnitude of the injection given on the right side of the panels. (For interpretation of the references in colour in this figure legend, the reader is referred to the web version of this article.)

With the example presented in Fig. 2, one sees that a key element to determine the real spatial distribution of the helicity flux density is the field line connectivity. The use of the helicity flux density (like G_A and G_θ) does not take into account such piece of information. In Pariat et al. (2005), we demonstrated that only the helicity rate per elementary flux tube (or per unit magnetic flux) is meaningful. A similar problem exists when trying to define the relative helicity density. In weakly inhomogeneous turbulence, Subramanian and Brandenburg (2006) have defined a helicity density using the concept of Gauss linking number and thus field line connectivity.

Let $\mathrm{d}h_\Phi/\mathrm{d}t|_e$ denote the helicity injected in the elementary flux tube e through its footpoints on the photosphere. Only this helicity rate per unit magnetic flux has a physical meaning. Nevertheless, it is possible to represent $\mathrm{d}\,h_\Phi/\mathrm{d}t|_e$ as a helicity flux density by distributing it between the footpoints of the elementary flux tube (which positions are denoted as $\mathbf{x}_{e_-}$ and $\mathbf{x}_{e_+}$)

$$\left.\frac{\mathrm{d}h_\Phi}{\mathrm{d}t}\right|_e = \frac{G_\theta(\mathbf{x}_{e_+})}{|\,B_n(\mathbf{x}_{e_+})\,|} + \frac{G_\theta(\mathbf{x}_{e_-})}{|\,B_n(\mathbf{x}_{e_-})\,|}. \tag{6}$$

$\mathrm{d}h_\Phi/\mathrm{d}t|_e$ is simply a field-weighted average of G_θ at both footpoints, and thus can be estimated using G_θ (provided that the field line connectivity is known).

The best surface helicity flux density proxies of $\mathrm{d}h_\Phi/\mathrm{d}t$, can be obtained by sharing $\mathrm{d}h_\Phi/\mathrm{d}t$ equally between the two footpoints of each elementary flux tube. One can use G_Φ , defined as (derived from Eq. (29) of Pariat et al., 2005, with f=1/2)

$$G_\Phi(\mathbf{x}_{e_\pm}) = \frac{1}{2}\left(G_\theta(\mathbf{x}_{e_\pm}) + G_\theta(\mathbf{x}_{e_\mp})\left|\frac{B_n(\mathbf{x}_{e_\pm})}{B_n(\mathbf{x}_{e_\mp})}\right|\right). \tag{7}$$

In the case of the magnetic flux tube rotating as a whole, when the number of turns is an integer, G_Φ does not present any polarity (see Fig. 2, bottom right panel). Directly on the G_Φ maps it is clear that no helicity is injected.

When the number of turns is not an integer, then G_Φ presents non-null polarities (Fig. 3). The reason is that inside each magnetic polarity, the G_θ distribution is not mirror symmetric with respect to the axis that passes through the center of the polarity and which is perpendicular to the main direction of the flux tube, e.g., the $\mathcal{S}$ axis shown in Fig. 2 (top right panel). This asymmetry is due to the fact that, two points in, e.g., the positive magnetic polarity do not rotate by the same amount with respect to a point in the negative magnetic polarity of the flux tube. In the positive polarity, the point which is closest to the negative polarity has a mean rotation rate $\mathrm{d}\theta/\mathrm{d}t$ (Eq. (4)) larger than any other point further away. Thus, when the number of turns is not an integer the asymmetry leads to non-null G_Φ.

Nevertheless, in the G_Φ map the polarities are real. The twist and the bending of the flux tube create an asymmetry between the elementary flux tubes linking the magnetic polarities if the number of turns is not an integer. More precisely, elementary flux tubes, starting at an equal distance from the center of a magnetic polarity, have a winding in the flux tube which depends on their azimuthal position in the polarity. As the flux tube rotates on itself, part of the elementary flux tubes are going below the axial field line $\mathcal{A}$ (which is untwisted) and the others are going above. This creates a redistribution of magnetic helicity inside the flux tube and thus some helicity flux at the boundary.

For a given field line, the sign of the helicity flux density depends on the sign of the rotation and of the mapping properties of field lines from one polarity to the other (so it depends on the twist modulo $[2\pi]$ and on its position relatively to the central field line $\mathcal{A}$).

For example, in Fig. 3, with the chosen rotation sign and a twist of half turn, the helicity flux density is positive in the right part and negative in the left part in each footpoint. Here locally non-null G_Φ polarity does not mean that some helicity is injected through the bottom boundary (photosphere). What G_Φ shows here is that some helicity is exchanged within the volume of the flux tube, between the field lines that are going under $\mathcal{A}$ and those that are going above. A similar case of redistribution of helicity has been presented in Pariat et al. (2005) when two polarities separate.

4. Analysis of an observational example

Even if only the helicity rate per unit of elementary magnetic flux has a physical meaning, to estimate $\mathrm{d}h_\Phi/\mathrm{d}t$ from observations, it is necessary to isolate flux tubes and determine their connectivity. With present observations this is actually not possible, and up to now, G_Φ could appear only as an theoretical tool. Nevertheless, thinking in terms of connectivity help us improve the study of the helicity flux

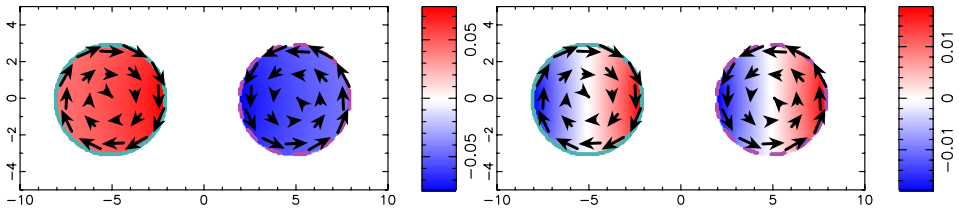

Fig. 3. Photospheric maps of G_θ (left panel) and G_Φ (right panel) for a twisted flux tube rotating as a whole, as in Fig. 2. The number of turns of the field line is equal to 0.5. The shading and arrow conventions are the same as in Fig. 2. Notice the difference in the injection magnitudes on the right side of the panels.

density done with G_θ. The study of active region AR 9182 illustrates how to go beyond G_θ. AR 9182 was previously studied by Nindos et al. (2003) and Pariat et al. (2006). Before October 9, 2000, it is formed by a positive compact leading sunspot and a more extended trailing negative spot. From October 9, magnetic flux emergence occurred west of the active region, in the form of two separating oppositely-signed magnetic polarities (see Fig. 4).

The original leading sunspot is the positive magnetic polarity noted as P_1 in Fig. 5 whereas the magnetic polarities of the emerging flux are indicated as N_2 and P_2. A magnetic polarity, due to projection effects, appears west of P_2. We will not take that area into consideration.

The G_A map (bottom left in Fig. 5) presents its usual complex patterns with several polarities of both signs. In the G_θ map most of these patchy patterns have disappeared. Three main areas of uniform sign remains on the main magnetic polarities: P_2 presents a wide negative G_θ whereas N_2 and P_1 have positive G_θ. G_θ reduces the fake polarities induced by G_A . The rates involved here are 41, -35 and 6.1×10^{21} Wb^2 s^{-1} for $(\mathrm{d}H_\theta/\mathrm{d}t)_+$, $(\mathrm{d}H_\theta/\mathrm{d}t)_-$ and $\mathrm{d}H_\theta/\mathrm{d}t$, respectively. From the G_θ map, one would conclude that there is simultaneous injection of helicity of both signs in the emerging flux (N_2 P_2).

Looking at the field evolution and the magnetic connectivity as traced by the observed coronal loops (Fig. 4), we suppose that the emerging polarities (N_2, P_2) in AR 9182 are magnetically connected and that they form a single flux tube. Then the real helicity rate injected in this flux tube will be the sum of the helicity injected through N_2 and P_2. But, since they have opposite values of G_θ with similar absolute intensities, the sign of $\mathrm{d}h_\Phi/\mathrm{d}t$ cannot be easily

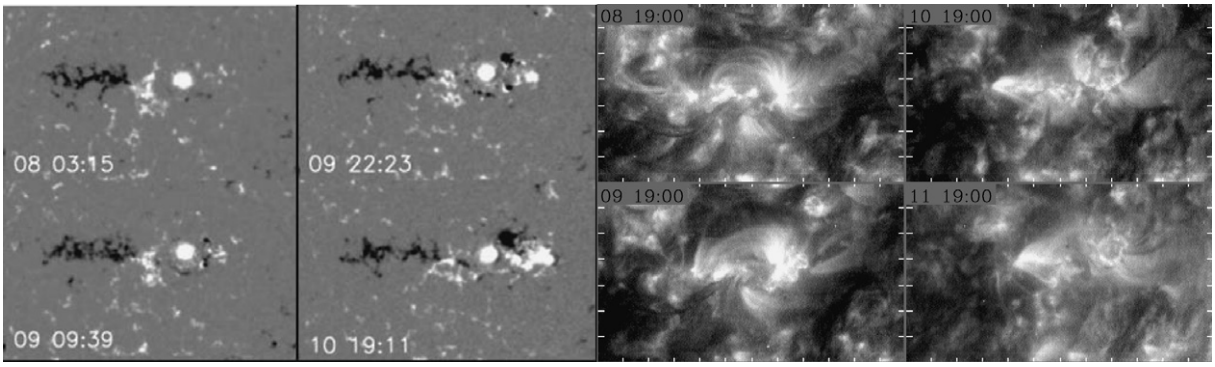

Fig. 4. Selected MDI magnetograms (left) and EIT/SoHO 171 Å filtergram images (right) showing the evolution of AR 9182 from October 8, 2000 to October 11. The panels are co-aligned to show the relationship between the photospheric and coronal evolution.

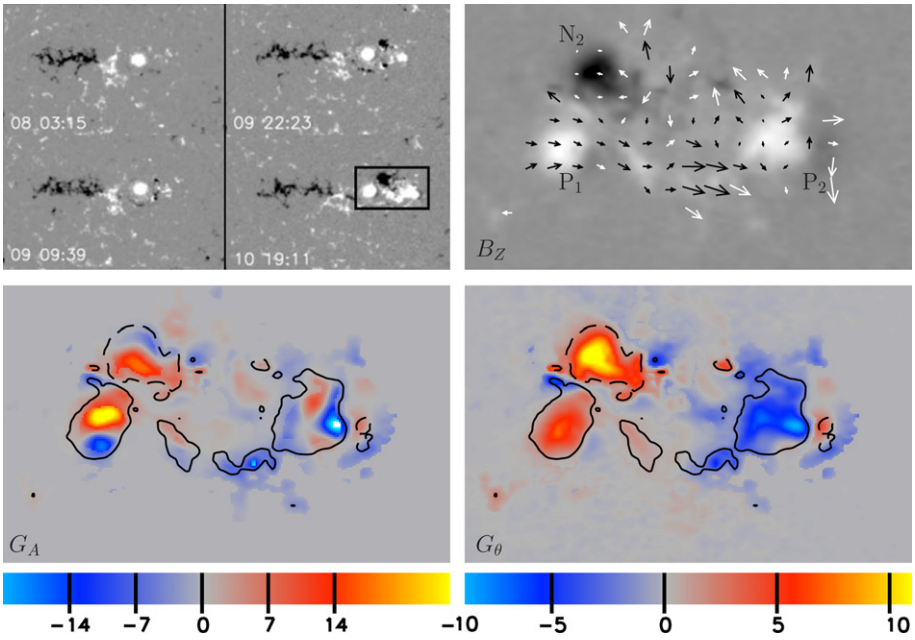

Fig. 5. Top left: selected MDI magnetograms of AR 9182 with white/black for positive/negative magnetic field, respectively. The black frame indicates the area that is enlarged in the other panels (emerging flux region). Top right: magnetogram on October 11, 2000 at 21:40 UT, with the computed LCT velocities. Bottom left: G_A map. Bottom right: G_θ map. The grey levels are in units of 10^6 Wb^2 m^{-2} s^{-1}. Two B_n isocontours are added for $B_n = \pm 300$ G.

deduced. This is why here G_θ fails to give an accurate picture of the real patterns of injected helicity. For this particular case, the properties of G_θ distribute the helicity injection over the footpoints in such a way that large fake polarities appear. To derive the helicity pattern one would need to derive G_Φ.

In order to have an idea of what G_Φ would give for AR 9182, we model this active region. We considered two flux tubes similar to the one used in the model of Fig. 2 (top left panel). These two half-toruses have the same small radius and field strength. The photospheric feet of the first flux tube correspond to the original pre-existing polarities. The second flux tube models the emerging magnetic flux (N_2 P_2). We assume that the flux tubes are not twisted. Our results confirms *a posteriori*, that it was not necessary to introduce any twist to obtain helicity patterns similar to the observed one. It implies that the inner twist of the flux tubes should inject relatively little helicity compared to the other motions. For simplicity, these torus-like flux tubes are represented when they are almost half-emerged, thus the sections of the tubes appear as circular regions, of opposite polarities.

This model also assumes that the magnetic polarities N_2 and P_2 are completely connected. This is obviously not the case in reality. Using SoHO/EIT (Delaboudiniere et al., 1995) images (see Fig. 4, right), we see that some UV loops are linking P_1 and N_2. Nevertheless, most of the loops still link P_2 with N_2. In addition, when looking at the evolution of AR 9182, the simultaneous appearance of P_2 and N_2 strongly suggests that these magnetic polarities are indeed the footpoints of a single emerging flux tube. We suppose that relatively little reconnection had occurred and changed the field connectivity between P_2 and N_2.

We implemented four kinds of motion to these flux tubes in order to match the main velocity pattern observed in AR 9182 : emergence, translation and rotation of the magnetic flux tube rooted in N_2 and P_2, and a translation motion for the flux tube rooted in P_1. The relative intensities of the motions were adjusted in order to fit as best as possible the observations, matching not only the velocity field but also the G_A and G_θ patterns.

With the above simple model we were able to derive G_A, G_θ and G_Φ. The results are presented in the last row in Fig. 6. Our model matches well the main polarities of G_A and G_θ observed in AR 9182. The model G_θ map, shows that negative density is located in P_2 whereas positive helicity flux density appears in N_2 and P_1. N_2 presents the largest helicity rate, as in the observations. The G_Φ map (bottom right in Fig. 6) gives a different result: the three magnetic polarities present positive helicity density.

In order to understand how the helicity is injected we computed G_A, G_θ and G_Φ separately for each implemented motion. The results are presented Fig. 6.

- First, we considered the vertical emergence of (N_2 P_2) (first row). This emergence creates an apparent separation of the footpoints of the flux tube. The horizontal velocity induced by the emergence is 1 (this motion defines the units of velocity). The total injected helicity is equal to 0.41 in normalized units of helicity rate (an helicity rate of 1 corresponds to the helicity injected by all the motions together). This motion creates intense fake signals in G_A and homogeneous injection with G_θ and G_Φ.
- Second, we considered a solid rotation of this whole flux tube, relatively to N_2 (second row). The velocity of this rotation is about 1.8. This motion is the only one that injects globally negative helicity : -0.25 units of helicity rate are injected. Even if the injection of helicity due to this motion is not globally dominant, it explains the negative rate of helicity observed in P_2 in the G_θ map. It is also responsible for the pattern associated with G_A in that polarity.
- Third, we imposed an eastward translational motion on this same emerging flux tube (third row), so that P_2 does not present any east-west motion when all the motions are summed. The total helicity injected is about 0.28 normalized units of helicity rate. In G_θ map this motion injects positive helicity in N_2 and P_1 and a small amount of negative helicity in P_2. Together with the emergence motion, they are at the origin of the helicity pattern observed in N_2 in the G_A map.
- Finally, for the flux tube rooted in P_1, we only considered a translation toward the west (fourth row). The relative velocity of this translation is 1.3 and the rate of helicity is about 0.56 units. Even if the velocity is not the biggest, this motion is the one that injects most of the helicity. Using G_A one would expect that the helicity is only injected through P_1. But G_θ and G_Φ maps show that the injection happens in both flux tubes. This is natural since the displacement of a flux tube relatively to another should inject helicity in both flux tubes.

The simultaneous implementation of these four motions (fifth row) gives a very good match between our model and the observations. Our model allows us to compute G_Φ and to infer the helicity injection. We found that the helicity injection is uniform in sign and relatively homogeneous. This results is consistent with what we previously found with the other studied active regions (Pariat et al., 2006).

5. Conclusion

In Pariat et al. (2005, 2006), we demonstrated with theoretical and observational examples how the usual proxy of magnetic helicity flux density, G_A (Eq. (3)), can produce spurious signals. We defined two new proxies of helicity flux density: G_θ (Eq. (4)), and G_Φ (Eq. (7)). The present paper extends and completes the interpretation and explanation of G_θ and G_Φ. In addition, we have developed the analysis of a pathological active region where G_θ creates strong fake polarities.

Indeed, although G_θ reduces efficiently spurious signals induced by G_A , G_θ can also present artifact polarities. In fact only the helicity rate per elementary flux tube, $\mathrm{d}h_\Phi/\mathrm{d}t$,

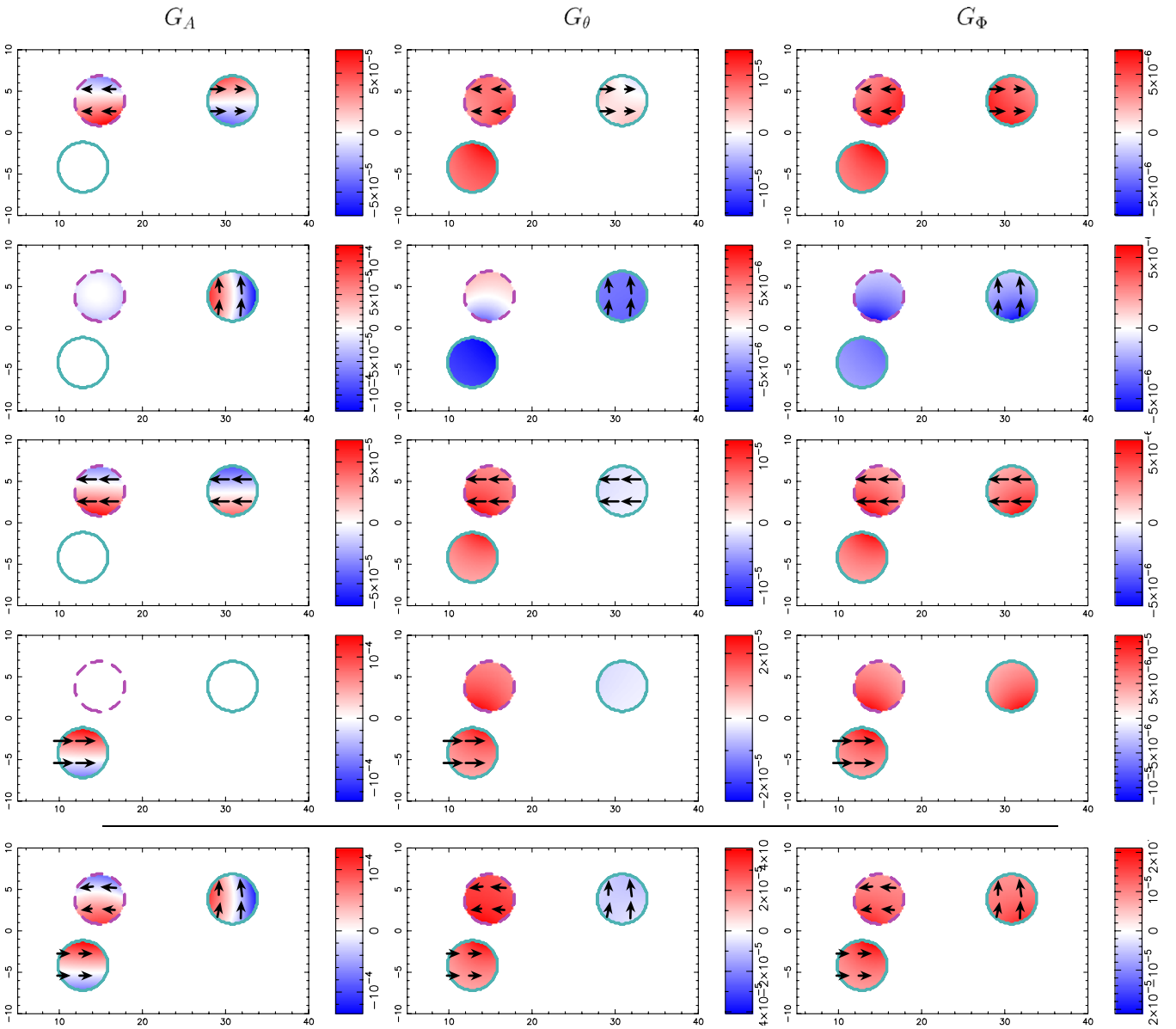

Fig. 6. Model maps of G_A (left column), G_θ (middle column) and G_Φ (right column) for each considered motions: emergence (first row), rotation (second row) and translation (third row) of (N_2 P_2); translation (4th row) of P_1. Fifth row: final model of AR 9182, summing the contributions of the above rows.

is physically meaningful and G_Φ is its best proxy. It is nevertheless difficult to use such quantity since it is necessary to determine the coronal linkage to compute G_Φ, which is presently not possible. In practice, G_θ is the best and simplest solution for mapping the injection of helicity. Even if it could induce spurious signals in some cases it is possible to infer the real patterns. For example, when two oppositely signed magnetic polarities which are believed to be linked present opposite G_θ signs, a better estimate of the real helicity flux density is an average of the helicity densities at these magnetic polarities.

AR 9182 is an example where G_θ creates intense unreal signals. In this AR the negative G_θ polarity in P_2 is only a fake signal if one supposes that P_2 and N_2 are linked. Thus even if G_θ sometimes produces fake signals, by a careful analysis, it is still possible to overcome this problem. Moreover, spurious G_θ signals are generally related to much weaker helicity flux density polarities. Understanding the coronal physics of, for example, flares and CMEs, needs the knowledge of the locations where magnetic helicity is injected. Such studies can thus benefit from G_θ looking forward to the possible systematic application of G_Φ.

Acknowledgements

E.P thank the ESA educational program for funding the travel, stay and participation to the 36th COSPAR meeting. We thank the two referees for their help in improving the manuscript. A.N was supported by Greek Ministry of Education's "Pythagoras II grant".

References

Antiochos, S.K., DeVore, C.R. The role of helicity in magnetic reconnection: 3D numerical simulations, in: Magnetic Helicity in Space and Laboratory Plasmas, pp. 187–196, 1999.

Berger, M.A. Rigorous new limits on magnetic helicity dissipation in the solar corona. Geophys. Astrophys. Fluid Dyn. 30, 79–104, 1984.

Berger, M.A. Magnetic helicity in space physics, in: Magnetic Helicity in Space and Laboratory Plasmas, pp. 1–9, 1999.

Berger, M.A. Topological quantities in magnetohydrodynamics. Adv. Nonlinear Dyn., 345–383, 2003.

Berger, M.A., Field, G.B. The topological properties of magnetic helicity. J. Fluid. Mech. 147, 133–148, 1984.

Brandenburg, A., Subramanian, K. Astrophysical magnetic fields and nonlinear dynamo theory. Phys. Rep. 417, 1–209, 2005.

Brown, M., Canfield, R., Pevtsov, A.Magnetic Helicity in Space and Laboratory Plasmas. Geophy. Mon. Ser, vol. 111. AGU, 1999.

Chae, J. Observational determination of the rate of magnetic helicity transport through the solar surface via the horizontal motion of field line footpoints. ApJ 560, L95–L98, 2001.

Chae, J., Wang, H., Qiu, J., Goode, P.R., Strous, L., Yun, H.S. The formation of a prominence in active region NOAA 8668. I. SOHO/MDI observations of magnetic field evolution. ApJ 560, 476–489, 2001.

Chae, J., Moon, Y., Park, Y. Determination of magnetic helicity content of solar active regions from SOHO/MDI magnetograms. Sol. Phys. 223, 39–55, 2004.

Chae, J., Jeong, H., Lim, E.K. Measurements of magnetic helicity injected through the solar photosphere, Adv. Space Res., in press, doi:10.1016/j.asr.2007.01.035, 2007.

Delaboudiniere, J.-P., Artzner, G.E., Brunaud, J., Gabriel, A.H., Hochedez, J.F., et al. EIT: extreme-ultraviolet imaging telescope for the SOHO mission. Sol. Phys. 162, 291–312, 1995.

Démoulin, P. Recent theoretical and observational developments in magnetic helicity studies, Adv. Space Res., in press, doi:10.1016/j.asr.2006.12.037, 2007.

Démoulin, P., Berger, M.A. Magnetic energy and helicity fluxes at the photospheric level. Sol. Phys. 215, 203–215, 2003.

Elsasser, W.M. Hydromagnetic dynamo theory. Rev. Mod. Phys. 28, 135–163, 1956.

Ji, H. Turbulent dynamos and magnetic helicity. Phys. Rev. Lett. 83, 3198–3201, 1999.

Kusano, K., Maeshiro, T., Yokoyama, T., Sakurai, T. Measurement of magnetic helicity injection and free energy loading into the solar corona. ApJ 577, 501–512, 2002.

Kusano, K., Maeshiro, T., Yokoyama, T., Sakurai, T. The trigger mechanism of solar flares in a coronal arcade with reversed magnetic shear. ApJ 610, 537–549, 2004.

Linton, M.G., Antiochos, S.K. Magnetic flux tube reconnection: tunneling versus slingshot. ApJ 625, 506–521, 2005.

Low, B.C. Solar activity and the corona. Sol. Phys. 167, 217–265, 1996.

Maeshiro, T., Kusano, K., Yokoyama, T., Sakurai, T. A statistical study of the correlation between magnetic helicity injection and soft X-ray activity in solar active regions. ApJ 620, 1069–1084, 2005.

Moffatt, H. The degree of knottedness of tangled vortex lines. J. Fluid Mech. 35, 117–129, 1969.

Moon, Y.-J., Chae, J., Choe, G.S., Wang, H., Park, Y.D., et al. Flare activity and magnetic helicity injection by photospheric horizontal motions. ApJ 574, 1066–1073, 2002a.

Moon, Y.-J., Chae, J., Wang, H., Choe, G.S., Park, Y.D. Impulsive variations of the magnetic helicity change rate associated with eruptive flares. ApJ 580, 528–537, 2002b.

Nindos, A., Zhang, H. Photospheric motions and coronal mass ejection productivity. ApJ 573, L133–L136, 2002.

Nindos, A., Zhang, J., Zhang, H. The magnetic helicity budget of solar active regions and coronal mass ejections. ApJ 594, 1033–1048, 2003.

Pariat, E., Démoulin, P., Berger, M.A. Photospheric flux density of magnetic helicity. A&A 439, 1191–1203, 2005.

Pariat, E., Nindos, A., Démoulin, P., Berger, M.A. What is the spatial distribution of magnetic helicity injected in a solar active region? A&A 452, 623–630, 2006.

Rust, D.M. Spawning and shedding helical magnetic fields in the solar atmosphere. Geophys. Res. Lett. 21, 241–244, 1994.

Subramanian, K., Brandenburg, A. Magnetic helicity density and its flux in weakly inhomogeneous turbulence. ApJ 648, L71–L74, 2006.